frontiers | Frontiers in Earth Science

TYPE Original Research
PUBLISHED 21 June 2023
DOI 10.3389/feart.2023.1204957

OPEN ACCESS

EDITED BY
Peng Tan,
CNPC Engineering Technology R&D Company Limited, China

REVIEWED BY
Cunfei Ma,
China University of Petroleum, Huadong, China
Zhaoxue Tian,
Tsinghua University, China

*CORRESPONDENCE
Shan Chen,
22361378@qq.com

RECEIVED 13 April 2023
ACCEPTED 12 June 2023
PUBLISHED 21 June 2023

CITATION
Li J, Tian Y, Chen S, Zhou H, Chi H, Ma Y and Kong L (2023), Pore types and microstructure of the black shale in the Lower Silurian, Southeast of Chongqing, China.
Front. Earth Sci. 11:1204957.
doi: 10.3389/feart.2023.1204957

Pore types and microstructure of the black shale in the Lower Silurian, Southeast of Chongqing, China

Juan Li[1,2], Yukun Tian[3], Shan Chen[1,2]*, Hui Zhou[1,2], Huanpeng Chi[1,2], Yanyan Ma[1,2] and Liyun Kong[1,2]

[1]Oil and Gas Survey, China Geological Survey, Beijing, China, [2]Unconventional Oil and Gas Geology Laboratory, China Geological Survey, Beijing, China, [3]Command Center of Natural Resources Comprehensive Survey, China Geological Survey, Beijing, China

The Lower Silurian black shale in the Southeast of Chongqing is of great potential in the accumulation of shale gas in South China. In order to understand the pore system of these black shales, mercury porosimetry, surface area study, mineralogy and image analyses by scanning electronic microscopy were performed. Four major pore types (interparticle pores, intraparticle pores, organic-matter pores and microfractures) were classified under the observation of the samples. Interparticle pores, which associate with mineral particles and mostly in micro-scale, can be subdivided into pores among rigid particles, ductile particles, and rigid-ductile particles. Intraparticle pores, which can be subdivided into cleavage-plane pores within clay minerals, intercrystalline pores within pyrite framboids and pores formed by partial or complete dissolution, are in nanometer scale and more common exist in unweathered rocks. Organic-matter pores are one type of intraparticle pores which are found within organic matter and appear to be prone to form effective networks and main permeable pathway. The rocks are abundant with microfractures where absorbed gas can be transformed to free gas. Microfractures which are partly cemented by residual organic residue are of great importance. Comparing the two sets of samples from Lujiao section and Well Yuye-1, we note that the outcrop samples from Lujiao section have much more interparticle pores than core samples, while the latter own more intraparticle pores. The results of quantitative and visual qualitative analyses about the gas shale reservoir pore system are similar. With the increasing of quartz, the number of interparticle pores and macropores increase. And intraparticle pores and micro-mesopores increase with clay minerals.

KEYWORDS

black shale, pore type, microfractures, Lower Silurian, Southeast of Chongqing

1 Introduction

Shale gas is an unconventional natural gas and is reserved in kerogen-rich black shale which is characterized by Low-porosity and low-permeability (Zhang et al., 2011 Yu et al., 2014; Zhang et al., 2022). Compared with conventional reservoir, gas shale itself is the source rock and the reservoir (Jiang et al., 2010; Wang et al., 2014; Ma et al., 2018; Liu et al., 2022). Shale gas can be found in free state within natural fractures and interparticle pores while a

significant part of shale gas can be found as the sorbed state within the kerogen and clay minerals (Li et al., 2013; Pu et al., 2022; Jiang et al., 2023).

At present, great progress has been made in the sedimentary environment, diagenesis and reservoir characteristics of black shale worldwide (Wang et al., 2009; Hammes et al., 2011; Milliken K L et al., 2013; Jiang et al., 2019; Nie et al., 2020; Sun et al., 2023).

Different from conventional experimental methods for reservoirs, quantitative methods such as surface, mercury intrusion, and pyknometer have significant advantages in studying shale reservoirs (Cui et al., 2012; Jia et al., 2017; Dong et al., 2022). Large pores can be seen with the naked eye and at low magnification, but there are still a large number of invisible micropores in the reservoir. Field emission scanning electron microscopy and environmental scanning electron microscopy for intuitive observation of nanoscale pore morphology and connectivity are highly favored by scholars.

During the last several years, a variety of pore types have been identified by researchers from the whole world. Loucks et al. (2012) divides pores into interparticle pores, intraparticles pores, organic-matter pores and fractures. Interparticle pores include pores between grains, pores between crystals, pore between clay platelets and pores at the edge of rigid grains. Intraparticle pores include intercrystalline pores within pyrite framboids, cleavageplane pores within clay, moldic pores and preserved intrafossil pores. During the research of Barnet Shale in north Texas and the Woodford Shale in southeastern Oklahoma, Slatt and Chalmers (Slatt and Brien, 2011; Chalmers et al., 2012; Huang et al., 2013) suggest that there are four main types of pores: interparticle pores produced by flocculation, organoporosity produced by burial and maturation, intraparticle pores from organisms, intraparticle pores within mineral grains and microchannels and microfractures. Liu et al. (2023) obtained nano-scale images through methods of argon Ion polishing-field emission scanning electron microscope observation and detected four pore types of shale reservoir including organic matter pores, mineral intergranular nano pores, mineral intragranular pores and micro-fractures.

On one hand, in foreign countries there has been a variety of research (Slatt and Brien, 2011; Chalmers et al., 2012; Loucks et al., 2012) about gas shales which are within low-middle maturity and in simple tectonic background using high-resolution field emission scanning electron microscopy. However, the Lower Silurian black shale in South China undergoes a long geological time with complex geological background and is rebuilded by many stages of tectonic activities. Therefore, this kind of high maturity shale has been observed less by high resolution SEMs. On the other hand, there has been lots of quantitative analyses including surface area, mercury porosimetry, isothermal adsorption intending to discuss the pore structure of gas shales in China (Li et al., 2012; Chen et al., 2013; Gao et al., 2020; Shao et al., 2022). But it's inadequate with visualization of pore systems, especially nanometer-scaled pores of the marine shale in South China. In order to make up the two shortage discussed above, high-resolution field emission scanning electron microscopy were used to investigate the pore types and characterization about the Lower Silurian black shale in South China in this paper. Expecting to document and present the pore characterization of the Lower Silurian black shale in South China and to make contribution to the exploration and development of unconventional shale gas in China.

2 Geological background and methods

In this investigation, data of pore types in the Lower Silurian black shale come from core and outcrop samples which are collected from Well Yuye-1 and Lujiao section in Pengshui county, Southeast of Chongqing province, China (Figure 1).

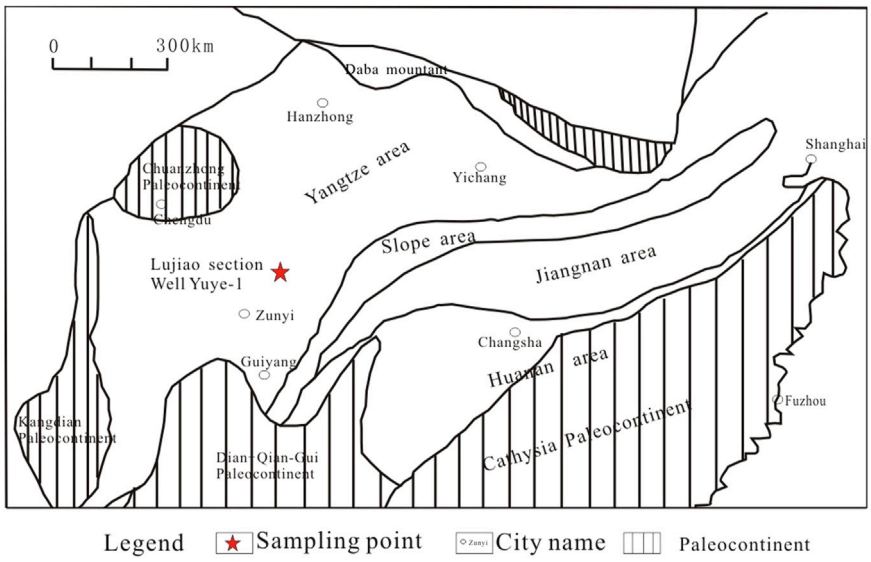

FIGURE 1
Paleogeography of the Late Ordovician to Early Silurian in Yangtze area.

TABLE 1 Statistics of mineral compositions and pore volume of Well Yuye-1 and Lujiao section, Southeast of Chongqing, China.

No.	Sample ID	Depth (m)	Quartz (%)	Orthoclase (%)	Albite (%)	Calcite (%)	Dolomite (%)	Pyrite (%)	Clay minerals (%)	TOC (%)	R_O (%)	Total pore volume (mL/g)	Micropore volume (mL/g)	Mesopore volume (mL/g)	Macropore volume (mL/g)
1	①-62	56。19	42	7	13	7	3	2	26	*	*	1.27E-02	5.69E-04	9.73E-03	2.40E-03
2	①-64	58.19	37	5	13	5	0	2	38	3.47	2.51	2.13E-02	1.56E-03	1.46E-02	5.10E-03
3	①-68	54.99	44	4	9	6	4	2	31	1.63	*	1.32E-02	1.38E-03	8.53E-03	3.29E-03
4	①-70	49.59	47	5	12	2	0	1	33	1.53	*	1.29E-02	1.27E-03	9.13E-03	2.50E-03
5	①-74	37.49	43	3	15	3	0	1	35	1.22	*	1.02E-02	9.79E-04	7.25E-03	1.97E-03
6	①-76	29.49	42	3	15	4	0	2	34	0.86	*	9.20E-03	8.55E-04	6.28E-03	2.07E-03
7	YY1-1260	126.0	32.7	0.3	6.9	1.8	2.8	2.3	53.2	1.02	1.93	5.10E-03	8.87E-04	3.77E-03	4.40E-04
8	YY1-1460	146.0	31.9	1.0	7.3	10.8	3.6	3.8	41.6	1.76	1.96	1.31E-02	8.31E-04	1.06E-02	1.70E-03
9	YY1-1660	166.0	35.7	4.2	10.2	3.6	2.0	3.4	40.9	1.35	2.10	7.00E-03	2.65E-04	5.77E-03	9.70E-04
10	YY1-1860	186.0	39.0	1.3	12.9	1.8	3.9	3.1	38.0	1.48	2.24	7.60E-03	5.41E-04	5.88E-03	1.18E-03
11	YY1-2050	205.0	37.7	2.0	11.0	6.7	6.4	10.6	25.6	1.45	2.21	7.40E-03	6.61E-04	5.11E-03	1.63E-03
12	YY1-2,148	214.8	49.4	2.7	17.1	5.8	3.7	3.9	17.4	1.18	2.13	5.80E-03	8.08E-04	3.79E-03	1.20E-03
13	YY1-2,372	237.2	46.1	4.6	11.0	0.8	3.0	3.6	30.9	1.63	1.92	6.50E-03	8.99E-04	4.92E-03	6.80E-04
14	YY1-2,657	265.7	53.0	1.0	8.8	5.1	4.7	3.2	24.2	2.29	2.26	8.60E-03	1.43E-03	4.40E-03	2.77E-03
15	YY1-2,850	285.0	40.7	3.1	16.5	0.1	6.6	3.0	30.0	1.38	2.00	6.30E-03	5.96E-04	4.80E-03	9.00E-04
16	YY1-3,170	317.0	39.8	1.0	10.5	2.3	5.1	2.9	38.4	1.75	1.89	8.80E-03	5.44E-04	7.34E-03	9.20E-04

Note: No. 1 to 6 belong to Lujiao section; No. 7 to 16 belong to Well Yuye-1; the symbol "*" stands for "not measured".

10.3389/feart.2023.1204957

10.3389/feart.2023.1204957

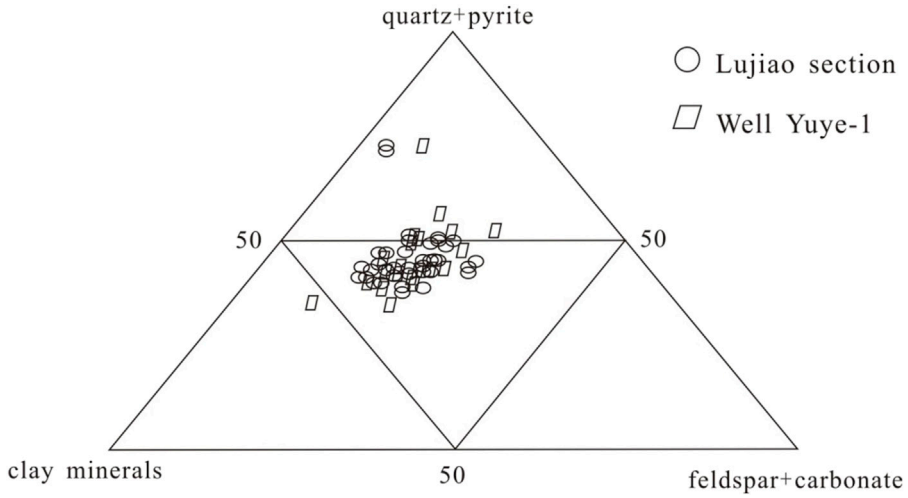

FIGURE 2
The mineralogical ternary diagram of the black shale in the Southeast of Chongqing.

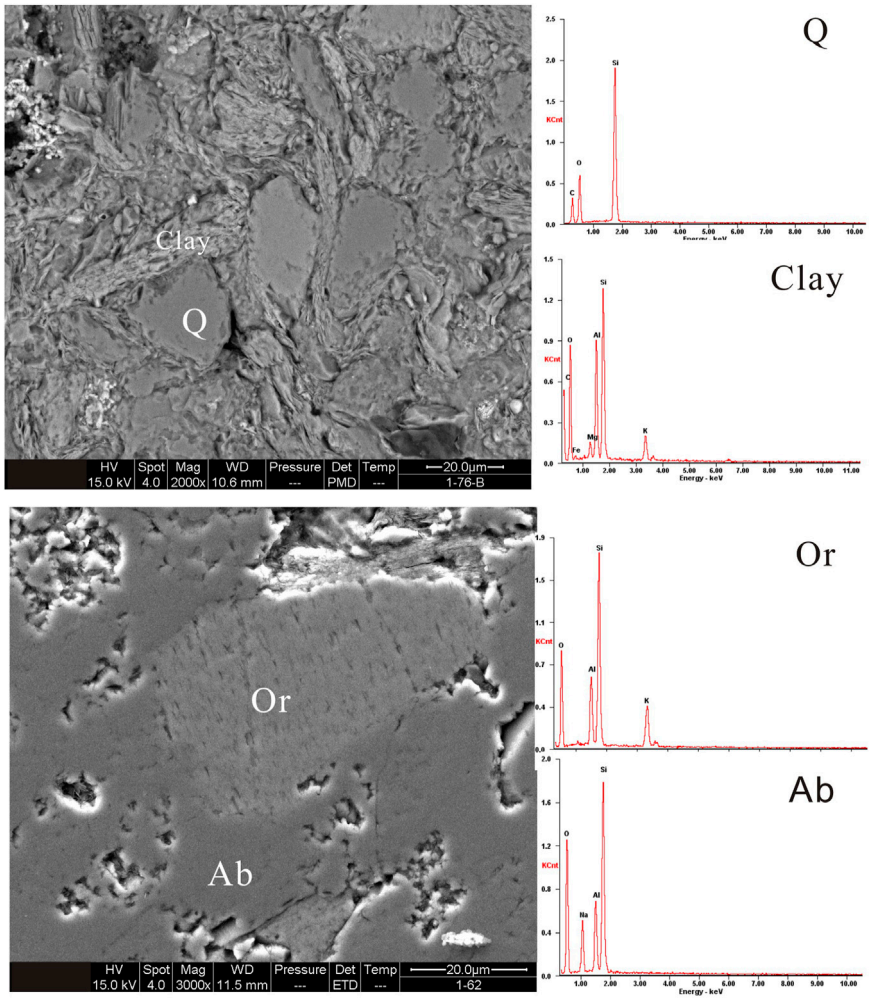

FIGURE 3
Field emission scanning electron microscope images of the main minerals in Longmaxi black shale. Note: Q=quartz, Clay=clay minerals, Or=Orthoclase, Ab=albite.

10.3389/feart.2023.1204957

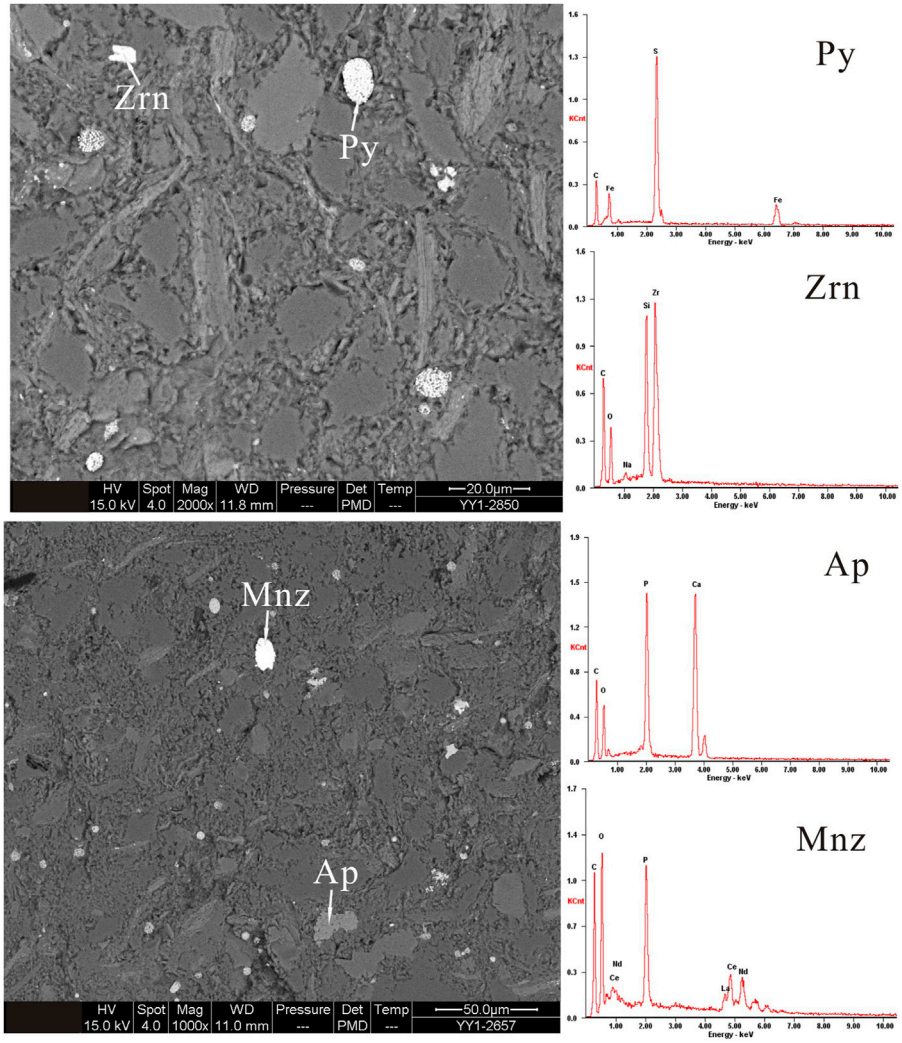

FIGURE 4
Field emission scanning electron microscope images of the accessory minerals in Longmaxi black shale. Note: Py=pyrite, Zrn=zircon, Ap=apatite, Mnz=monazite.

The outcrop strata of Lujiao section are well-exposed and the formation interfaces among Wufeng formation, Longmaxi formation and Luoreping formation are distinct. The target layer is Longmaxi formation with the thickness of 63.19 m and lithology of black shale and black pelitic siltstone. The depth of Well Yuye-1 is 350 m and the target layer is Longmaxi formation of the Lower Silurian with the mainly lithology of black shale and thin interbed of mudstone and siltstone.

117 samples were obtained from Lujiao outcrop section and 39 samples were analyzed. 21 samples were obtained from drill cuttings in Well Yuye-1. As the depth of the test samples increases, the upper part is basically evenly spaced, and the target layer is encrypted for testing. Analysis and study on mineralogy, vitrinite reflectance, TOC, physical property and surface area were performed on each sample. 16 samples were analyzed by field emission scanning electron microscopy and energy dispersive spectrometry (Table 1). Variaty information such as numbers of samples, accelerating voltage, magnification and scale bar can be found on the SEM-micrograph data bar.

Mineralogical composition analysis was performed by Research Institute of Petroleum Exploration and Development OF North China. Based on the two standards of SY/T 5163-1995 and SY/T 5983-94, samples were analyzed by D8 DISCOVER X-Ray diffraction at the temperature of 24°C and relative humidity of 35%.

Samples were examined by two different types of field-emission SEMs. One is an FEI Quanta 200 FEG in the State Key Laboratory of Tribology, TsingHua University and the other is a ZESS SUPRA 55 in the State Key Laboratory of Bio-geology and Environmental geology, China University of Geosciences. FE-SEM can work in high vacuum, rough vacuum and normal environment. Combined with the latest X-ray energy dispersive spectroscopy, it can be used in the observation and analysis of mushy material and thin film, absorption phenomenon of chemical modified particle in rough vacuum environment. In order to improve the electrical conductivity of the samples and acquire high-quality images, all

TABLE 2 Classification of gas shale reservoir comparing different references with this paper.

names	Pore types												
	Interparticle pores				Intraparticle pores						Organic-matter pores	Fracture pores	
Loucks et al. (Loucks et al., 2012)	Pores between grains	Pores between crystals	Pores between clay plateles	Pores at the edge of rigid grains	Intercrystalline pores within pyrite framboids	Intraplatelet pores within clay aggregates	Pores within peloids or pellets	Dissolution-rim pores	Pores within fossil bodies	Moldic pores after a crystal	Moldic pores a fossil	microchannels and microfractures	
Slatt et al. (Slatt and Brien, 2011)	porous floccules		organopores		fecal pellets			fossi fragments		intraparticle grains/pores			
Wu et al. (Wu et al., 2012)	porous floccules	pores of organic matter fossils	asphalt pores from organic matter debris		pores of pyrite grain	intercystal pores within mineral grains	microchannels	microfractures		pores from calcium fossils		pores between the debris surrounding rock	
This text	pores between rigid particles	pores between rigid and ductile particles	pores between ductile particles		cleavage-plane pores within clay minerals		intercrystalline pores within pyrite framboids		pores formed by dissolution		organic-matter pores	microfractures	
	interparticle pores				intraparticle pores								

Note: see text for detail.

samples were coated with 10 nm carbon. Many excellent photographs were acquired through secondary electron and backscattered secondary electron. Also energy dispersive spectroscopy analyses of specific grains were conducted for mineral identification. When imaging with BSEs, different atomic number shows different brightness. Usually, the kerogen is discernible by its darker gray-scale value while metal minerals are white and clay, quartz and carbonate are light gray.

Based on the two national standards of GB/T 19145-2003 and GB/T 18602-2001, TOC were measured by Carbon and Sulfur Determinator and Oil and Gas Evaluation Instrument at the temperature of 27°C.

Based on the standard of SY/T5336—1996, physical properties of the rocks were examined by Ultrapore-200A Helium porosimeter and ULTRA-PERMTM 200 permeameter at the temperature of 23°C, the humidity 50% and the barometric pressure of 1025 hPa.

The capillary pressure curve analysis and surface area analysis were also performed by Research Institute of Petroleum Exploration and Development in North China based on related standards.

3 Results of mineralogy

According to the X-Ray diffraction analyses, the black shales in Lujiao section are rich in quartz (44%) and clay (38%), with a small amount of feldspar (18%), and illite is in the dominant position among all clay minerals. In Well Yuye-1, the main minerals are also quartz (39%) and clay minerals (33%), while both of them are a little smaller in amount ratio compared with Lujiao section. However, there are more pyrite and carbonate (7.3%) in Well Yuye-1 (Table 1).

The apices are (1) quartz and pyrite, (2) carbonate and feldspar, and (3) clay minerals (Figure 2). Quartz and pyrite are relatively stable in chemical and mechanical state for their rigid grains and generally not undergoing dissolution. Carbonate and feldspar are also rigid grain, but they are chemically unstable and forms moldic pores easily. Clay minerals are ductile grains and easily deformed, so they are also unstable in mechanical and chemical state.

Based on the images of field emission scanning electron microscopy, we found that the main minerals in these observed samples are quartz, clay and feldspar (Figure 3), and the accessory minerals are pyrite, zircon, apatite, and so on (Figure 4). These results are consistent with the X-ray diffraction analysis.

4 Classification of pores

According to the observed images by field emission scanning electron microscopy, a simple and descriptive approach to grouping mudstone pores into four basic categories is been proposed which is on the basis of their relationships with particles. These pores are interparticle pores, intraparticle pores, organic-matter pores and microfractures. Furthermore, interparticle pores are subdivided into pores between rigid particles, pores between rigid and ductile particles, and pores between ductile particles. Intraparticle pores include cleavage-plane pores within clay minerals, intercrystalline pores within pyrite framboids, and pores formed by partial or complete dissolution (Table 2).

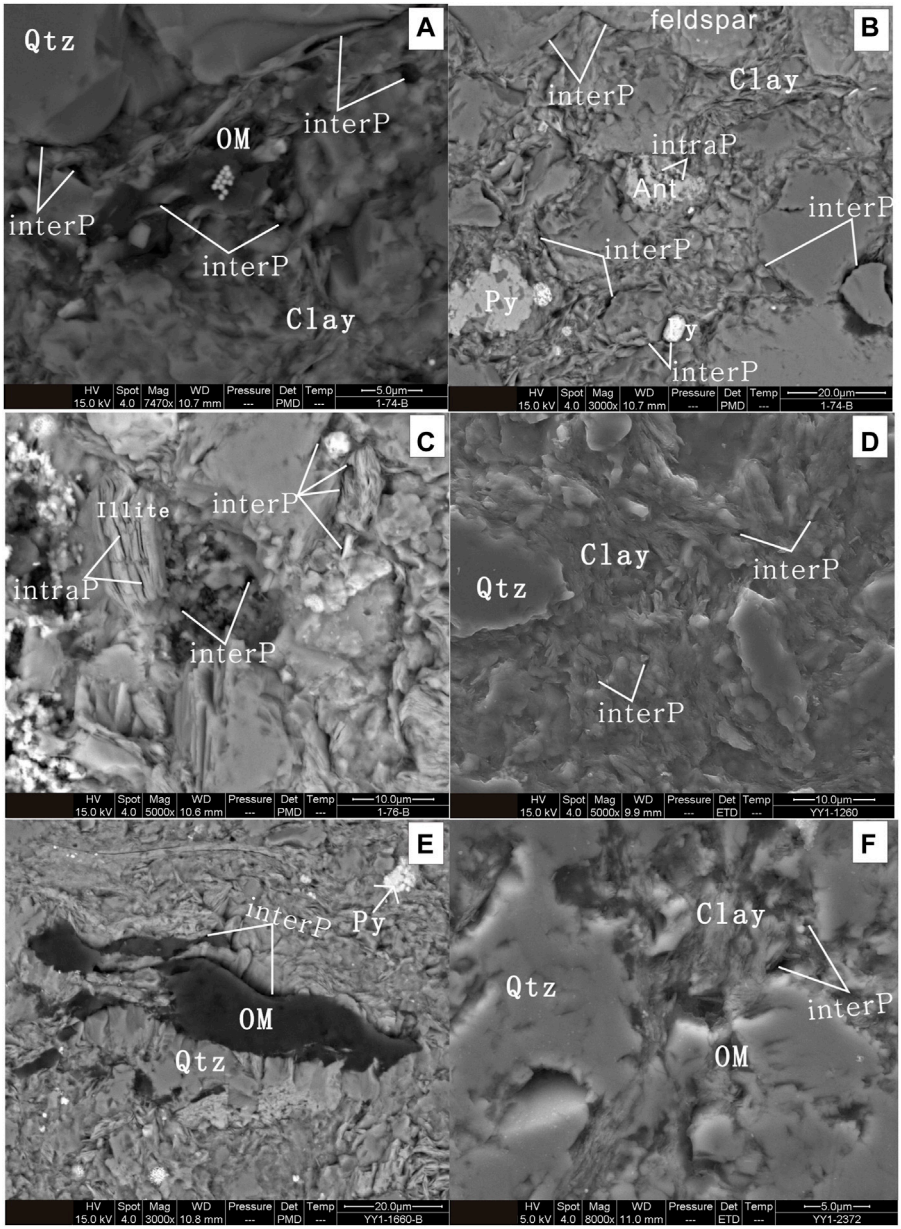

FIGURE 5
Field emission scanning electron microscope images of interparticle pores in Longmaxi black shale. Note: **(A,B)** TOC=1.22, from Lujiao outcrop section; **(C)** TOC=0.86, from Lujiao outcrop section; **(D)** TOC=1.02, Ro=1.93%, from Well Yuye-1; **(E)** TOC=1.35, Ro=2.10%, from Well Yuye-1; **(F)** TOC=1.63, Ro=1.92%, from Well Yuye-1; OM=Organic Matter; Qtz=Quartz; Py=pyrite; interP=interparticle pore; intraP=intraparticle pore; WD=Working distance; HV=high voltage.

4.1 Interparticle pores

Interparticle pores occur between rigid particles or ductile particles and are commonly well connected, forming effective pore networks. Examples of ductile particles are clay flocculates, mica, and organic matter; examples of rigid particles are quartz, feldspar, and pyrite.

Through the observation of samples collected from outcrop section and drill, it can be found that pores between rigid particles are mainly pores between quartz (Figure 5A; Figure 3B), pores between quartz and feldspar (Figure 5B), pores between quartz and pyrite (Figure 5B) and so on. Similarly, pores between ductile and rigid particles include pores between quartz and clay minerals (Figures 5C,D,F), pores between quartz and organic matter (Figure 5A,E), pores between pyrite and organic matter (Figure 5A,C), pores between pyrite and clay minerals (Figure 5B) and so on. Pores between ductile particles are pores between clay minerals (Figure 5C,D) and pores between clay minerals and organic matter (Figure 5A,E).

Interparticle pores are complex in shape and appear not to show a strong preferential orientation. These pores range from nanometer scale to micrometer scale, commonly in micrometer scale which are

10.3389/feart.2023.1204957

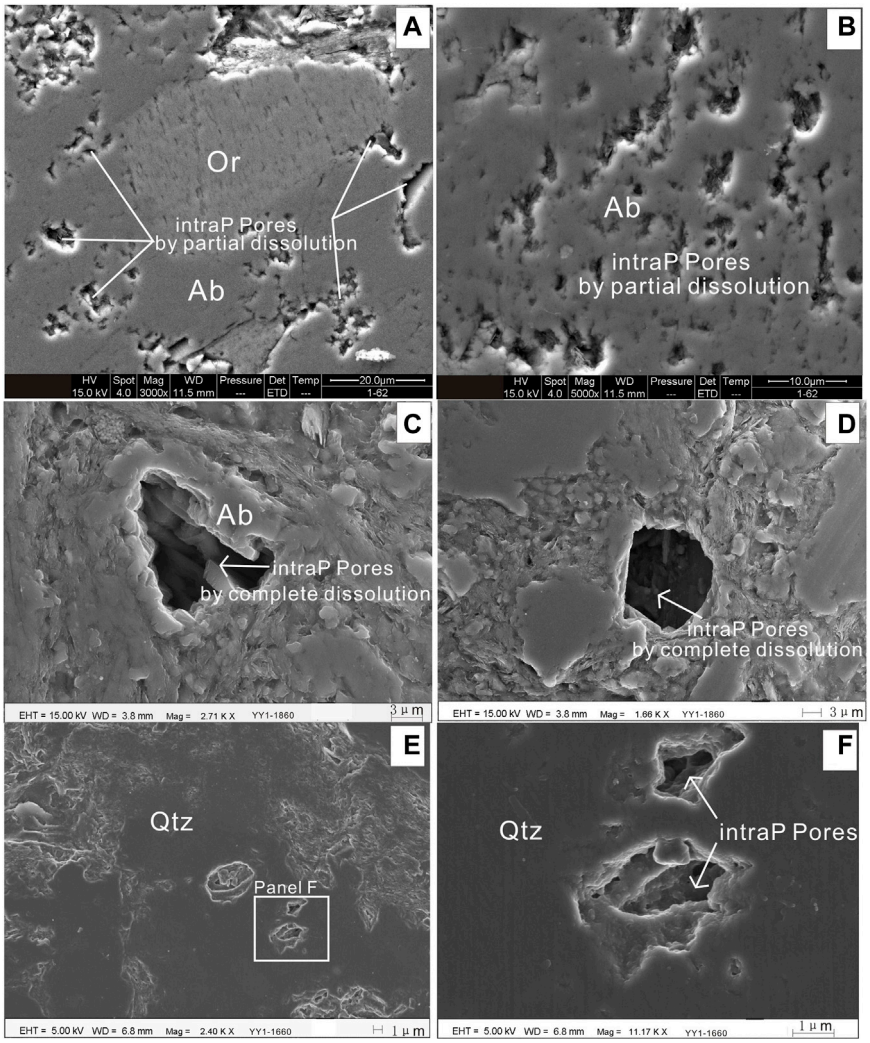

FIGURE 6
Field emission scanning electron microscope images of intraparticle pores in Longmaxi black shale (1). Note: **(A,B)** abundant of feldspar, from Well Yuye-1; **(C,D)** TOC=1.48, Ro= 2.24%, from Well Yuye-1; **(E,F)** TOC=1.35, Ro=2.10%, from Well Yuye-1; F is the close-up view of **(E)**.

concentrated around rigid grains such as quartz and pyrite (Figure 5). From the very beginning, interparticle pores are abundant and in micrometer scale in majority. During the time, ductile grains are distorted and flow into interparticle pores between rigid grains, adding to the loss of interparticle pore space, so most pores became nanometer scale (Figure 5F).

Figure 5A shows interparticle pores occur commonly between quartz and organic matter, have lengths in the 1-μm range, and are in elongated shape. Figure 5B shows abundant interparticle pores between rigid grains. Figure 5C shows effective connectivity between illite taking the shape of thin slice. In Figure 5D, it can be found that compared to outcrop samples, core samples have much less interparticle pores because of compaction and cementation. Usually these pores are scattered with no strong preferential orientation. Sometimes, parts of the pores are triangular in shape which interpreted to be the remaining pore space between compacted and cemented rigid grains (Loucks et al., 2012). Figure 5E shows some interparticle pores between organic matter and quartz or clay minerals which are in micrometer scale and present elongated shape. These pores guarantee the channel between organic-matter pores and mineral pores and make the gas produced by organic matter transported to mineral pores which are of great importance to the migration and production of shale gas.

4.2 Intraparticle pores

Intraparticle pores within mineral grains range from simple to complex in shape and with different origins. A small amount of the pores are primary formed at beginning, while the majority was formed in diagenetic processes. The main types of intraparticle pores are cleavage-plane pores within clay minerals, intercrystalline pores within pyrite framboids, and pores formed by partial or complete dissolution (Figures 6, 7).

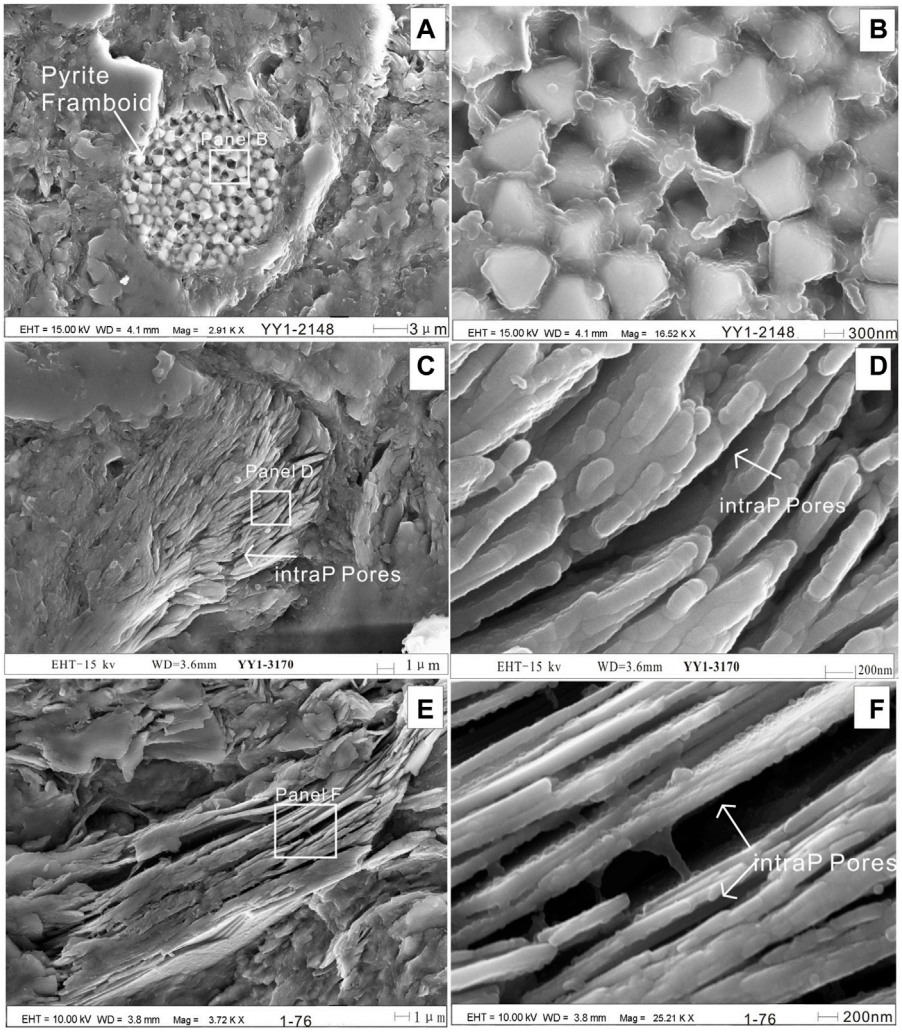

FIGURE 7
Field emission scanning electron microscope images of intraparticle pores in Longmaxi black shale (2). Note: **(A,B)** TOC=1.18, Ro= 2.13%, from Well Yuye-1; **(C,D)** TOC=1.75, Ro= 1.89%, from Well Yuye-1; **(E,F)** from Lujiao outcrop section; B, D and F are the close-up view of **(A,C,E)** respectively.

Undergoing a long geological history and mechanical compaction, most primary pores are destroyed or cemented (Rouquerol et al., 1994). However, abundant dissolution pores formed in the latter time (Figure 6). Actually, dissolution pores are intraparticle pores resulted from the process of carbonate, apatite and feldspar dissolution and reprecipitation. In this paper, pores resulted from the dissolution of feldspar are very abundant in most observed samples. These pores are irregular in shape and different in size (Figures 6A,B). Some of the dissolution pores are filled by illite, others are open and with the size of 5 μm which are more common in core samples compared with the outcrop samples (Figures 6C,D). In addition, pores resulted from the dissolution of quartz are also been found with relatively small size which is about 1 μm (Figures 6E,F).

In core and outcrop samples, there is abundant intraparticle space within pyrite framboids, especially when pyrite crystals were detached by outside forces (Figures 7A,B). The space within pyrite framboids contains clay or residual organic mucus, or nothing.

Research shows that the shape of intraparticle pore is generally controlled by its origin (Kanitpanyacharoen et al., 2012) which is suitable to cleavage-plane pores within clay minerals. In clay particles, especially illite, intraparticle pores are sheetlike and are parallel to one another with the size of smaller than 200 nm. In addition, residual organic mucus is commonly found around some clay minerals (Figures 7C,D,E,F).

4.3 Organic-matter pores

Pores within organic matter are called organic-matter pores (OM pores) in this article. Compared with core samples, outcrop samples have less organic matter and organic-matter pores because of weathering, although there are considerable organic-matterpores in both core samples and outcrop samples (Figures 8, 9). Organic-matter pores commonly exist in samples which come from drill cuttings (Figure 9). Usually with the drilling depth goes deeper, the number of

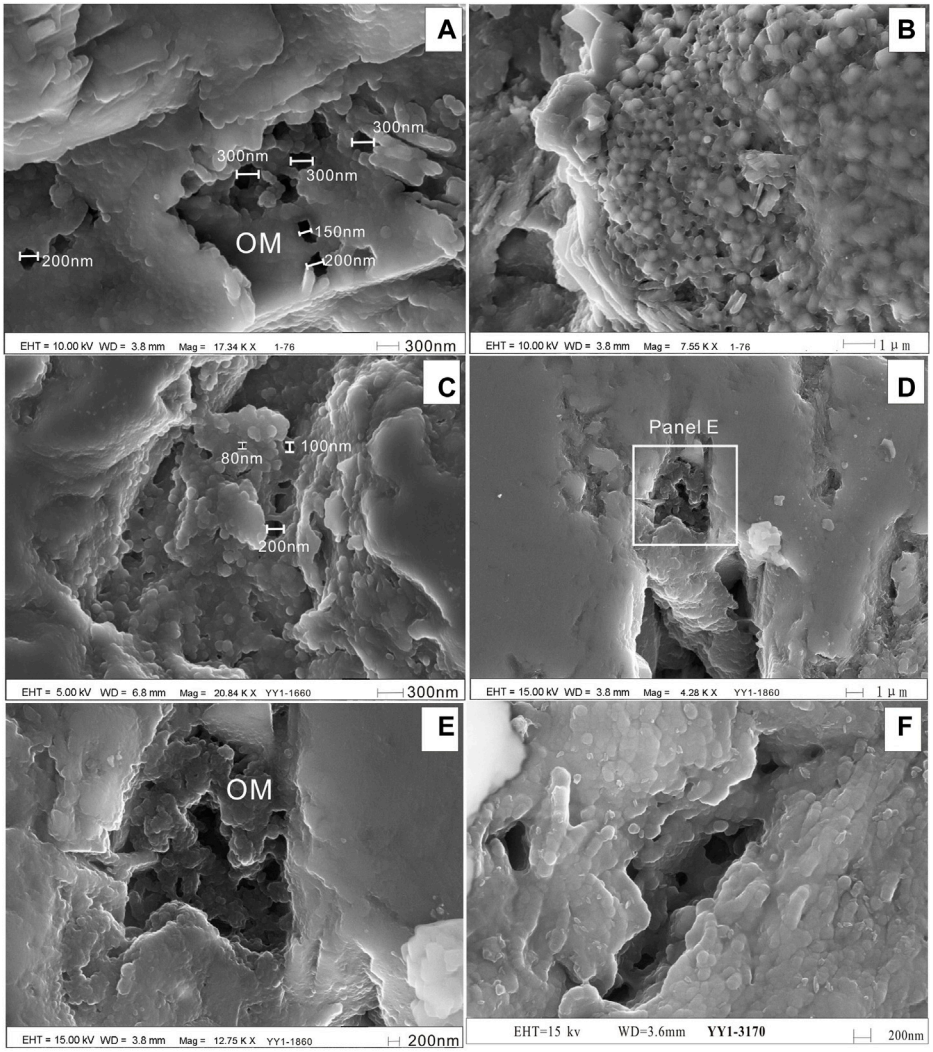

FIGURE 8
Field emission scanning electron microscope images of Organic-matter pores in Longmaxi black shale (1). Note: **(A,B)** from Lujiao outcrop section; **(C)** TOC=1.35, Ro=2.10%, from Well Yuye-1; **(D,E)** TOC=1.35, Ro=2.10%, from Well Yuye-1; **(F)** TOC=1.75, Ro=1.89%, from Well Yuye-1; E is the close-up view of **(D)**.

organic-matter pores shale increase. In addition, some organic mucus is found around pyrite framboids as said above (Figure 7B; Figure 8B).

Some organic-matter pores occur as absorbed coatings around clay grains and form abundant pores which are smaller than 100 nm scale. Published experimental and observational studies indicate that although these pores are not connected to each other in two-dimensional space, while in three-dimensional space their connectivity is perfect and has high value to shale gas reservoir (Nie and Zhang, 2011).

4.4 Microfractures and microchannels

Microfractures and microchannels have a significant effect on shale gas system (Pitman et al., 2001; Gale and Holder, 2010), especially in hydrocarbon production. The scale of microfractures rangsfrom nanometer to micrometer and the fractures can have a strong influence on the impermeability of tight rocks. The existence of some cemented fractures may deeply effect induced fracture propagation.

In the process of hydrocarbon production, with internal pressure increases gradually there emerges more microfractures. When the numbers of microfractures reach sufficient quantity, these microfractures offer storage space and permeability pathways for hydrocarbon to through the shales (Slatt and Brien, 2011).

By field emission scanning microscopy, we have the opportunity to observe microfractures in various sizes and shapes clearly in core samples and outcrop samples. These microfractures are commonly in micrometer scale and almost exist in all samples (Figure 10). Some of them are open and less than 500 nm in width with sinuous and discontinuous structure (Figures 10A,B). Some microfractures are cemented by clay minerals and exist between the space of rigid grains such as quartz (Figure 10E,F). Previous studies show that quartz is one of the factors which have strong influence on microfractures. Also, some microfractures are filled with bitumen

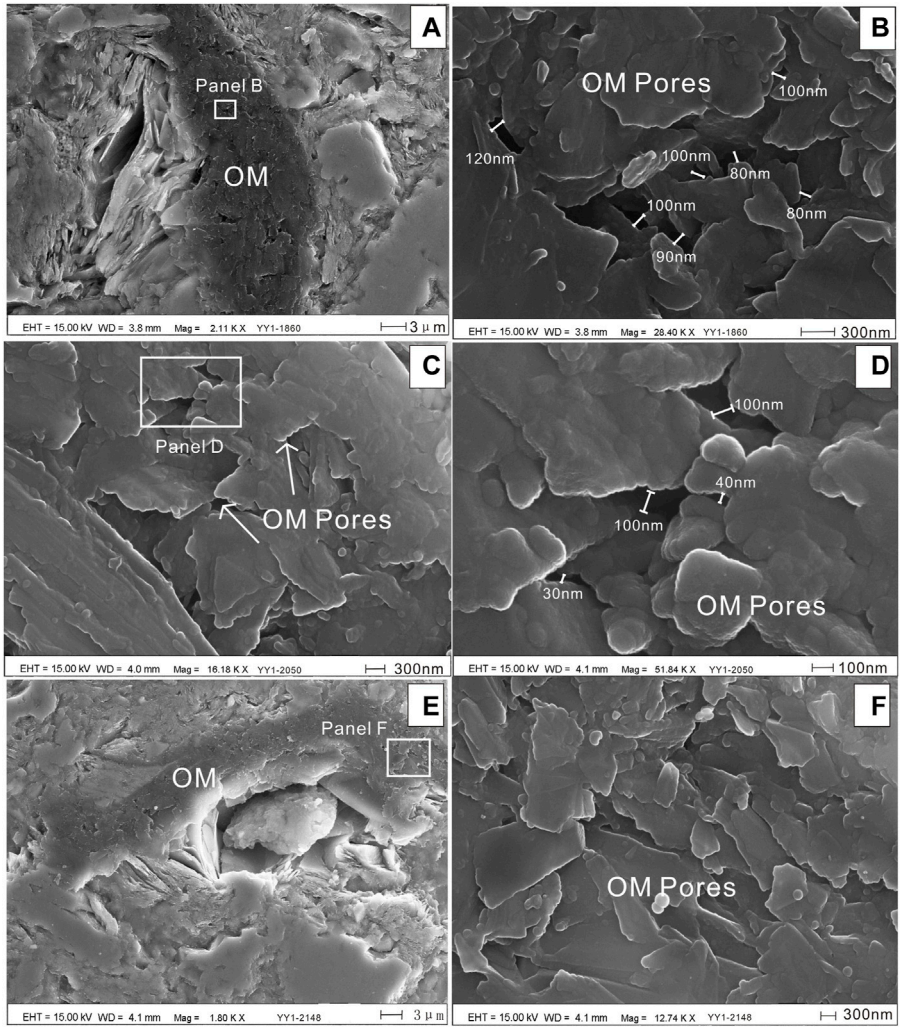

FIGURE 9
Field emission scanning electron microscope images of Organic-matter pores in Longmaxi black shale (2). Note: **(A,B)** TOC=1.35, Ro= 2.10%, from Well Yuye-1;**(C,D)** TOC=1.02, Ro= 1.93%, from Well Yuye-1; **(E,F)** TOC=1.18, Ro= 2.13%, from Well Yuye-1; **(B,D,F)** are the close-up view of **(A,C,E)** respectively.

with pyrite around (Figures 10C,D). All the microfractures above are wide enough to provide a permeability pathway for gas molecules which are of significant importance.

5 Discussion

5.1 Characteristic of pore type and structure

In the process of studying shale gas, some researchers (Loucks et al., 2009; Yang et al., 2022) suggest that there are two major unanswered questions: (1)where is the gas stored in the rock and (2) what pathway does the gas follow from the matrix to these induced fractures that allow it to flow into the well bore. To address these questions, we need to investigate pore structure present in this unit. As we all know, pore structure, which usually means the shape, size, distribution and microstructure of pore and pore throat, is of great importance to gas production and gas storage in shale gas exploration.

The images above indicate that the diameter of interparticle pores commonly range from several nanometers to a few micrometers (Figure 5). Intraparticle pores are subdivided into two categories from the perspective of pore size: dissolution pores are in micrometer scale (Figure 6) while cleavage-plane pores within clay minerals and intercrystalline pores within pyrite framboids are in nanometer scale (Figure 7). Organic-matter pores are in nanometer scale and smaller than intraparticle pores in size range (Figures 8,9). Therefore, shale-gas reservoir of the Longmaxi Formation in southeastern Chongqing is mainly nanometer pores with small amount of micrometer to millimeter pores.

In shallow-buried mudrocks, interparticle pores are relatively abundant in both rigid grains and ductile grains and have good connectivity. As rocks are buried and exposed over time to high temperature and pressure, they become

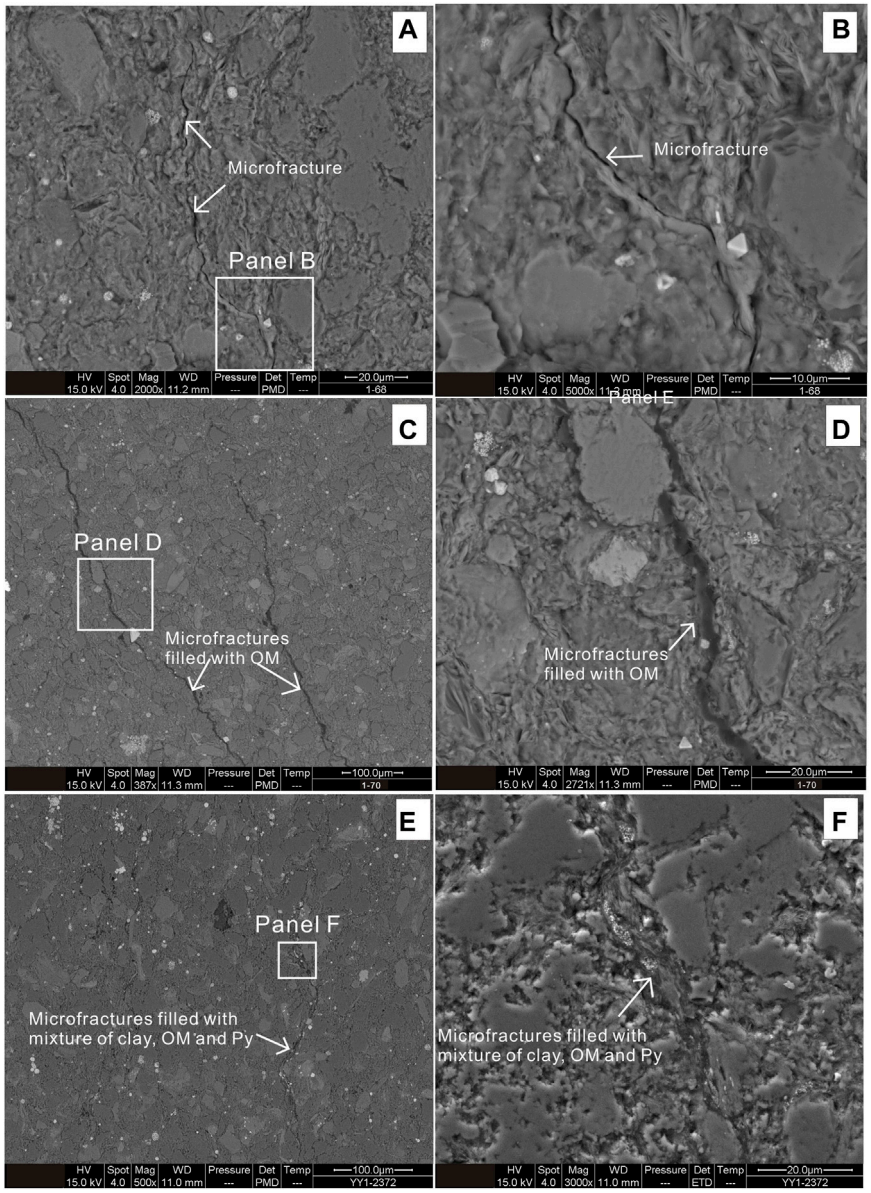

FIGURE 10
Field emission scanning electron microscope images of microfractures in Longmaxi black shale. Note: **(B,D,F)** are the close-up view of **(A,C,E)** respectively.

lithified and have less pores because ductile grains are distorted and flow into interparticle pores between rigid grains, blocking pore space and throats and adding the loss of interparticle pores (Loucks et al., 2012). This phenomenon is very obvious from observed samples. Comparing the two sets of samples from Lujiao section and Well Yuye-1, we note that the outcrop samples from Lujiao section have much more interparticle pores than the core samples from Well Yuye-1 (Figure 5). This is because compaction is more clear in core samples than outcrop samples, leading to the change of interparticle pores in quantity and size (Jin, et al., 2011).

Although core samples do not have interparticle pores as many as outcrop samples, they own most intraparticle pores such as cleavage-plane pores within clay minerals, intercrystalline pores within pyrite framboids, and pores formed by partial or complete dissolution (Figures 6, 7) which is caused by special temperature and pressure. Also we found that most intraparticle pores are filled with organic mucus (Figure 7). Loucks et al. (2009) holds the opinion that these pores are isolated and disconnected from each other which is not good for shale gas reservoir. However, others (Curtis et al., 2012) suggest that organic mucus have a strong adsorbability to gas and clay minerals have a large internal surface area (Zhong, 2012) which can store lots of gas and are of great importance. In addition, this kind of pores looks disconnected in two-dimensonal but actually connected in three-dimensonal demonstrated by many researchers.

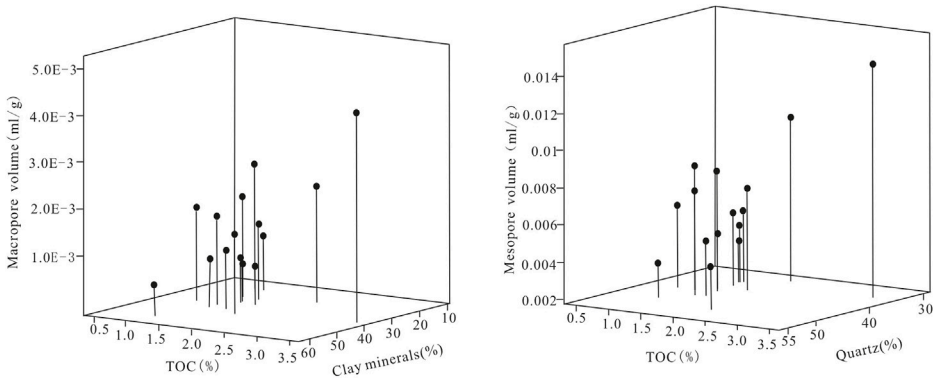

FIGURE 11
Relation between the content of TOC, clay minerals, quartz and pore volume of black shale.

The maturity of Longmaxi samples is over 1.9% and TOC is over 1.6%, so organic matter pores is quite common in most samples (Figures 8,9). The research of organic-matter pores are gradually valued in the study of shale gas basins in America (Nix and Burkhardt, 2003; Loucks et al., 2009; Chalmers et al., 2012; Modica and Lapierre, 2012). Usually organic matter pores form like this: during the diagenetic processes, following the increasing temperature and pressure, organic matter becomes porous and these pores provide places for generated gases. In this paper, we observed organic matter pores in different shape and commonly are in nanometer scale. Organic-matter pores can form an effective pore system and the dominate flow pathway.

5.2 Relationship between pore types and minerals

When studying the pore characteristics of the early Silurian Longmaxi Formation shale in northwestern Hunan, Yang (2022) believed that the development degree of micropores was mainly controlled by organic matter content. Mesopores with a pore size of 2–40 nm were mainly contributed by organic matter pores and clay minerals, while pores with a pore size greater than 40 nm were closely related to intergranular pores formed by quartz and other minerals. Quantitative analysis (Li et al., 2012; Huang et al., 2022) has shown that with increasing clay minerals, micropore and mesopores volumes relatively increase whereas macropore volumes decrease. An inverse relationship exists between clay minerals and quartz. With increasing quartz, volumes of micropore and mesopores relatively decrease whereas macropore volumes increase (Figure 11). These quantitative results are consistent with the observed images by field emission scanning electron microscopy.

Most interparticle pores are distributed between detrital minerals with the size of macroscale. So with the increasing of quartz, macropores increase. Interparticle pores usually exist between clay minerals except dissolution pores. Therefore, with the increasing of clay minerals, micro to meso pores increase.

In addition, research of the low to middle maturity shale abroad has identified that interparticle pores are mostly macropores and have a close relationship with quartz while micro to meso pores have a close relationship with clay minerals and organic matter (Slatt and Brien, 2011; Loucks et al., 2012; Chalmers et al., 2012). Thus, there are similarities and difference between low-middle maturity shale abroad and high maturity shale in South China.

6 Summary and conclusion

(1) According to the observed images by field emission scanning electron microscopy, we propose a simple and descriptive approach to grouping mudrock pores into four basic categories on the basis of their relationships with particles. These pores are interparticle pores, intraparticle pores, organic-matter pores and microfractures.

(2) The scale of interparticle pores arecommonly in micrometer scale. Intraparticle pores are different in size scale: dissolution pores are in micrometer scale while cleavage-plane pores within clay minerals and intercrystalline pores within pyrite framboids are in nanometer scale. Usually, organic matter pores are in nanometer scale and in order of magnitude smaller than intraparticle pores. So, the reservoir of shale is mostly nanometer pores with a small number of millimeter to micrometer pores.

(3) In shallow-buried mudrocks, interparticle pores are relatively abundant and have good connectivity. Comparing the two sets of samples, we note that the outcrop samples from Lujiao section have much more interparticle pores than the core samples from Well Yuye-1. This is because in core samples compaction is clearer than in outcrop samples, which leads to the change of interparticle pores in quantity and size. Core samples own most intraparticle pores such as cleavage-plane pores within clay minerals, intercrystalline pores within pyrite framboids, and pores formed by partial or complete dissolution because of special temperature and pressure.

(4) Both quantitative and visual qualitative analyses of the gas shale reservoir pore system are similar to each other. With the increasing of quartz, interparticle pores and macropores increase. intraparticle pores and micro-mesopores increase with clay minerals.

Data availability statement

The original contributions presented in the study are included in the article/Supplementary Material, further inquiries can be directed to the corresponding author.

Author contributions

JL: Investigation, writing—original draft. YT: Sample analysis, software. HZ: Review and editing. SC: Data analysis, methodology, writing. HC: Formal analysis, review and editing. YM: Writing—review and editing. LK: Review, editing and validation. All authors contributed to the article and approved the submitted version.

Funding

This research is supported by the three Projects of Investigation and evaluation of shale gas in key basins (DD20230023), Investigation and Evaluation of CO_2 Geological Storage and Utilization Potential in Oil and Gas Enrichment Areas (DD20230025), and the Enrichment Conditions and Favorable Area Selection of Coalbed Methane in Southern Sichuan to Western Guizhou.

Conflict of interest

JL, SC, HZ, HC, YM, and LK were empolyed by Oil and Gas Survey.

The remaining author declares that the research was conducted in the absence of any commercial or financial relationships that could be construed as a potential conflict of interest.

Publisher's note

References

Chalmers, G. R., Bustin, R. M., and Power, R. M. (2012). Characterization of gas shale pore systems by porosimetry, pycnometry, surface area, and field emission scanning electron microscopy/transmission electron microscopy image analyses: Examples from the barnett, Woodford, haynesville, marcellus, and doig units. *AAPG Bull.* 96 (6), 1099–1119. doi:10.1306/10171111052

Chen, W., Zhou, W., Luo, P., Deng, H., Li, X., Shan, R., et al. (2013). Analysis of the shale gas reservoir in the lower silurian Longmaxi Formation, changxin 1 well, Southeast sichuan basin,China. *Acta Petrol. Sin.* 29 (3), 1073–1086.

Cui, J., Zou, C., Zhu, R., Bai, B., Wu, S., and Wang, T. (2012). *New Adv. shale porosity Res. Adv. Earth Sci.* 27 (12), 319–325.

Curtis, M. E., Sondergergeld, C. H., Ambrose, R. J., and Rai, C. S. (2012). Microstructural investigation of gas shales in two and three dimensions using nanometer-scale resolution imaging. *AAPG Bulletion* 96 (4), 665–677. doi:10.1306/08151110188

Dong, D., Liang, F., Guan, Q., Jiang, Y., Zhou, S., Yu, R., et al. (2022). Development model and identification evaluation technology of Wufeng- Longmaxi Formation quality shale gas reservoirs in the Sichuan Basin. *Nat. Gas. Ind.* 42 (8), 96–111. doi:10.3787/j.issn.1000-0976.2022.08.008

Gale, J. F. W., and Holder, J. (2010). Natural fractures in some U.S. Shales and their importance for gas production. *Pet. Geol. Conf. Ser.* 7, 1131–1140. doi:10.1144/0071131

Gao, B., Liu, Z., Shu, Z., Wu, Y., Cao, M., Ju, S., et al. (2020). Gut microbiota in early pregnancy among women with Hyperglycaemia vs. Normal blood glucose. *Oil gas Geol.* 41 (2), 284–194. doi:10.1186/s12884-020-02961-5

Hammes, U., Hamlin, H. S., and Ewing, T. E. (2011). Geologic analysis of the Upper Jurassic Haynesville shale in east Texas and west Louisiana. *AAPG Bull.* 95 (10), 1643–1666. doi:10.1306/02141110128

Huang, J., Huang, Z., Liu, L., Li, X., Hu, H., Guo, W., et al. (2022). Pore size characterization and their mainly controlling factors in Wulalike formation shale, Ordas Basin. *J. Central South Univ. Technol.* 53 (9), 3418–3433. doi:10.11817/j.issn.1672-7207.2022.09.011

Huang, Z., Chen, J., Xue, H., Wang, Y., Wang, M., Deng, C., et al. (2013). Design, synthesis and biological evaluation of novel mansonone E derivatives prepared via CuAAC click chemistry as topoisomerase II inhibitors. *Songliao Basin :Petroleum Explor. Dev.* 40 (1), 58–71. doi:10.1016/j.ejmech.2013.07.011

Jia, C., Jia, A., and Han, P. (2017). Reservoir characterization and development evaluation of organic-rich gas-bearing shale layers in the Lower Silurian Longmaxi Formation Sichuan Basin. *Nat. Gas. Geosci.* 28 (9), 1406–1415. doi:10.11764/j.issn.1672-1926.2017.07.007

Jiang, P., Wu, J., Zhu, Y., Zhang, D., Wu, W., and Zhang, R. (2023). Enrichment conditions and favorable areas for exploration and development of marine shale gas in Sichuan basin. *Acta Pet. Sin.* 44 (1), 91–109. doi:10.7623/syxb202301006

Jiang, Y., Dong, D., Qi, L., She, Y., Jiang, C., He, F., et al. (2010). A novel mechanism of cell growth regulation by Cell Cycle and Apoptosis Regulatory Protein (CARP)-1. *Nat. Gas. Ind.* 30 (10), 7–12. doi:10.1186/1750-2187-5-7

Jiang, Y., Fu, Y., and Xie, J. (2019). Development trend of marine shale gas reservoir evaluation and a suitale comprehensive evaluation system. *Nat. Gas. Ind.* 39 (10), 1–9. doi:10.3787/j.issn.1000-0976.2019.10.001

Jin, L., Rother, G., Cole, R. D., Mildner, D. F., Duffy, C. J., and Branrley, S. L. (2011). Characterization of deep weathering and nanoporosity development in shale-a neutron study. *Am. Mineralogist* 96, 498–512. doi:10.2138/am.2011.3598

Kanitpanyacharoen, W., Kets, F. B., Wenk, H. R., and Wirth, R. (2012). Mineral preferred orientation and microstructure in the posidonia shale in relation to different degrees of thermal maturity. *Clays clay minerals* 60 (3), 315–329. doi:10.1346/ccmn.2012.0600308

Li, J., Yu, B., Zhang, J., Li, Y., Wu, J., Hakendorf, P., et al. (2012). Prevalence of resuscitation orders among residents from aged care facilities admitted to general medical units. *Oil Gas Geol.* 33 (3), 364–374. doi:10.1111/j.1447-0594.2011.00774.x

Li, Y., Liu, H., Zhang, L., Lv, Z., Li, Q., and Huang, Y. (2013). Lower limits of evaluation parameters for the lower Paleozoic Longmaxi shale gas in southern Sichuan Province:Science China. *Earth Sci.* 56, 710–717. doi:10.1007/s11430-013-4579-4

Liu, D., Wang, M., Zhao, T., Lu, H., Chen, X., and Guan, X. (2023). Classification and quantitative characterization of nano-scale pore structure in shale reservoirs of wufeng-longmaxi formation: A case study of well WX-1 in wuxi area. *Unconv. oil gas* 10 (1), 93–103. doi:10.19901/j.fcgyq.2023.01.12

Liu, Z., Wang, P., Nie, H., Li, P., and Li, Q. (2022). Enrichment conditions and favorable prospecting targets of Cambrian shale gas in Middle-Upper Yangtze. *J. central south Univ. Technol.* 53 (9), 3694–3707. doi:10.11817/j.issn.1672-7207.2022.09.031

Loucks, R. G., Reed, R. M., Ruppel, S. C., and Hammes, U. (2012). Spectrum of pore types and networks in mudrocks and a descriptive classification for matrix-related mudrock pores. *AAPG Bull.* 96 (4), 1071–1098. doi:10.1306/08171111061

Loucks, R. G., Reed, R. M., Ruppel, S. C., and Jarvie, D. M. (2009). Morphology, Genesis, and distribution of nanometer-scale pores in siliceous mudstones of the Mississippian Barnett shale. *J. Sediment. Res.* 79 (12), 848–861. doi:10.2110/jsr.2009.092

Ma, Y., Cai, X., and Zhao, P. (2018). China's shale gas exploration and development: Understanding and practice. *Petroleum Explor. Dev.* 45 (4), 589–603. doi:10.1016/s1876-3804(18)30065-x

Milliken, K. L., Rudnichi, M., David, N., and Zhang, T. (2013). Organic matter-hosted pore system, Marcellus Formation(Devonian), Pennsylvania. *AAPG Bull.* 97 (2), 177–200. doi:10.1306/07231212048

Modica, C. J., and Lapierre, S. G. (2012). Estimation of kerogen porosity in source rocks as a function of thermal transformation: example from the Mowry Shale in the Powder River Basin of Wyoming. *AAPG Bulletion* 96 (1), 87–108. doi:10.1306/04111110201

Nie, H., He, Z., and Liu, G. (2020). Genetic mechanism of high quality shale gas reservoirs in the Wufeng-Longmaxi Fms in Sichuan Basin. *Nat. Gas. Ind.* 40 (6), 31–41. doi:10.3787/j.issn.1000-0976.2020.06.003

Nie, H., and Zhang, J. (2011). Types and characteristics of shale gas reservoir: a case study of Lower Paleozoic in and around Sichuan Basin. *Pet. Geol. &Experiment* 33 (3), 219–225.

Nix, T., and Burkhardt, S. F. (2003). New methods applied to the microstructure analysis of Messel oil shale: confocal laser scanning microscopy (CLSM) and environmental scanning electron microscopy (ESEM). *Geol. Mag.* 140 (4), 469–478. doi:10.1017/s0016756803008094,v.

Pitman, J. K., Price, L. C., and LeFever, J. A. (2001). *Diagenesis and fracture development in the Bakken Formation, Williston Basin; implications for reservoir quality in the middle member U. S.* Geological Survey Professional Paper, 19.

Pu, B., Dong, D., Guan, Q., Jiang, S., Guo, W., and Zhang, S. (2022). Analysis of main controlling factors for the enrichment and high productivity of the Longmaxi shale gas in Southern Cichuan basin. *Geophys. Prospect. petroleum* 61 (5), 918–928. doi:10.3969/j.issn.1000-1441.2022.05.016

Rouquerol, J., Avnir, D., Fairbridge, C. W., Everett, D. H., Haynes, J. M., Pernicone, N., et al. (1994). Recommendations for the characterization of porous solids (Technical Report). *Int. Union Pure Appl. Chem. Pure Appl. Chem.* 68, 1739–1758. doi:10.1351/pac199466081739

Shao, D., Zhang, Y., Song, H., Meng, K., Luo, H., Li, Y., et al. (2022). Discussion on reservoir characteristics and main controlling factors of the Cambrian shale in Middle-Upper Yangtze region. *J. Northwest Univ. Sci. Ed.* 52 (6), 997–1012. doi:10.16152/j.cnki.xdxbzr.2022-06-008

Slatt, R. M., and Brien, N. R. (2011). Pore types in the Barnett and Woodford gas shales:contribution to understanding gas storage and migration pathways in fine-grained rocks. *AAPG Bull.* 95 (12), 2017–2030. doi:10.1306/03301110145

Sun, J., Liu, G., Shi, P., Xue, P., Liu, C., and Xu, J. (2023). Reservoir characteristics and analysis of shale gas resource potential in Shanxi Formation in Yan'an area. *Unconv. oil &gas* 10 (1), 44–51. doi:10.19901/j.fcgyq.2023.01.06

Wang, L., Zou, C., Zheng, P., Chen, S., Zhang, Q., Xu, B., et al. (2009). Geochemical evidence of shale gas existed in the Lower Paleozoic Sichuan basin. *Nat. Gas. Ind.* 29 (5), 59–62. doi:10.3787/j.issn.1000-0976.2009.05.011

Wang, X., Gao, S., and Gao, C. (2014). Geologiacl features of Mesozoic continental shale gas in south of Ordos Basin, NW China. *Petroleum Explor. Dev.* 41 (03), 294–304. doi:10.11698/PED.2014.03.04

Wu, J., Yu, B., and Li, Y. (2012). An improved high performance liquid chromatography-fluorescence detection method for the analysis of major phenolic compounds in cigarette smoke and smokeless tobacco products. *J. Southwest Petroleum Univ. Science Technol. Ed.* 34 (4), 40–47. doi:10.1016/j.chroma.2012.09.060

Yang, X., Tan, J., and Hu, R. (2022). Characterization of pore structure of shale reservoir of early Silurian Longmaxi Formation in northwest Hunan. *Unconv. oil gas* 9 (5), 25–35. doi:10.19901/j.fcgyq.2022.05.03

Yu, Y., Zou, C., Dong, D., Wang, S., Li, J., Yang, H., et al. (2014). Geological Conditions and Prospect Forecast of Shale Gas Formation in Qiangtang Basin, Qinghai-Tibet Plateau. *Acta Geol. Sin. Engl. Ed.* 88 (02), 598–619. doi:10.1111/1755-6724.12217

Zhang, J., Bian, R., Jin, T., Tang, X., Yin, T., Zhang, Q., et al. (2011). Fundamental significance of gas shale theoretical research. *Geol. Bull. China* 30 (2-3), 318–323.

Zhang, J., Zhou, Z., Song, T., Li, F., Chen, R., Lu, Y., et al. (2022). Comparison of exploration and development history, geological characteristics and exploitation conditions of shale gas in China and the United States and its enlightenment. *Acta Pet. Sin.* 43 (12), 1687–1701. doi:10.7623/syxb202212002

Zhong, T. (2012). Characteristic of pore structure of marine shales in South China. *Nat. Gas. Ind.* 32 (9), 1–4. doi:10.3787/j.issn.1000-0976.2012.09.001